

# Effect of the Liquid–Liquid Phase Separation on the Crystallization Behavior of a Poly(ethylene-*ran*-vinyl acetate) and Paraffin Wax Blend

JIN KON KIM, BYOUNG-KEE KIM, MINSOO PARK

Department of Chemical Engineering, Polymer Research Institute, Electronic and Computer Engineering Divisions, Pohang University of Science and Technology, Pohang, Kyungbuk 790-784, Korea

Received 2 February 1999; revised 13 December 1999; accepted 13 December 1999

**ABSTRACT:** The effect of liquid–liquid phase separation (LLPS) on the crystallization behavior of poly(ethylene-*ran*-vinyl acetate) with a vinyl acetate content of 9.5 wt % (EVA-H) in the critical composition of a 35/65 (wt/wt) EVA-H/paraffin wax blend was investigated by small-angle light and X-ray scattering methods and rheometry. This blend exhibited an upper critical solution temperature (UCST) of 98°C, and an LLPS was observed between the UCST and the melting point of 88°C for the EVA-H in the blend. As the duration time in the LLPS region increased before crystallization at 65°C, both the spherulite size and the crystallization rate of the EVA-H increased, but the degree of the lamellar ordering in the spherulite and the degree of crystallinity of the EVA-H in the blend decreased. © 2000 John Wiley & Sons, Inc. *J Polym Sci B: Polym Phys* 38: 707–715, 2000

**Keywords:** liquid–liquid phase separation; crystallization; lamellar ordering; phase behavior; EVA/wax blends

## INTRODUCTION

Semicrystalline/semicrystalline polymer blend systems, such as poly(ethylene oxide)/poly(hydroxybutyrate),<sup>1</sup> poly(vinylidene fluoride)/poly(1,4-butylene adipate),<sup>2–4</sup> isotactic poly(propylene)/isotactic poly(1-butene),<sup>5</sup> and poly( $\beta$ -hydroxybutyrate)/poly(vinyl acetate-*co*-vinyl alcohol)<sup>6</sup> blends, exhibit a complicated phase behavior. Although some researchers have investigated the effect of liquid–liquid phase separation (LLPS),<sup>7–10</sup> which can occur in a molten state, its effect on the crystallization behavior of semicrystalline/amorphous polymer blends has not been studied in detail because the LLPS is not determined easily due to its competition with the crystallization. Of course, a semicrystalline/semicrystalline polymer blend becomes a semicrystalline/amorphous polymer blend when the blend is investigated at tempera-

tures larger than the melting point of one component in the blend.

Previously, we reported that a blend of poly(ethylene-*ran*-vinyl acetate) (EVA-H) and paraffin wax showed an LLPS at temperatures higher than the melting points of both polymers.<sup>11</sup> Also, this LLPS affected the crystallization behavior of the EVA-H in the blend and the mechanical properties of the blend. Specifically, as the duration time at the LLPS region increased, both the degree of the crystallinity of the EVA-H in the blend and the flexural modulus decreased.<sup>11</sup> In this study, we investigated in detail the effect of the LLPS on the crystallization behavior of the EVA-H in the molten wax state by using differential scanning calorimetry (DSC), a light scattering method, wide-angle and small-angle X-ray scattering methods, and rheometry.

## EXPERIMENTAL

### Materials

The blend employed in this study consisted of EVA-H and paraffin wax. The vinyl acetate con-

Correspondence to: J. K. Kim (E-mail: jkkim@postech.ac.kr)

*Journal of Polymer Science: Part B: Polymer Physics*, Vol. 38, 707–715 (2000)  
© 2000 John Wiley & Sons, Inc.

**Table I.** Molecular Characteristics of the Materials

Sample Code	$M_n$	$M_w$	$M_z$	$M_w/M_n$	$M_z/M_w$	$T_m$ (°C)	Density (g/cc)
EVA-H (9.5% vinyl acetate)	21,000	74,800	154,800	3.56	2.07	95	0.930
Paraffin wax	540	560	580	1.04	1.03	55	0.900

$M_n$  = number-average molecular weight;  $M_w$  = weight-average molecular weight;  $M_z$  =  $z$ -average molecular weight.

tent in the EVA-H was 9.5 wt %. Table I gives the molecular weights and polydispersities of the EVA-H and wax as determined by high-temperature gel permeation chromatography (Waters Co. GPC-150C) with polyethylene.<sup>11</sup>

### Calorimetric Measurements

The degree of crystallinity and the melting endotherm ( $\Delta H_m$ ) of the EVA-H in the blend as well as those of the neat EVA-H were measured by DSC (Perkin–Elmer DSC 7 series). Prior to measurement, the baseline was established with two empty pans. To prevent thermal degradation, nitrogen gas was circulated around the sample pan. Each sample of about 10 mg first was heated at a heating rate of 10°C/min from 10 to 130°C and maintained at this temperature for 3 min to ensure that all blends became homogeneous. Then, the sample was cooled to 65°C after three different cooling histories: (1) direct quenching from 130 to 65°C, (2) an LLPS at 95°C for 20 min followed by quenching to 65°C, and (3) an LLPS at 95°C for 1 h followed by quenching to 65°C. Hereafter, these cooling histories are referred to as cooling protocols I, II, and III, respectively. Then, the blend was crystallized isothermally at 65°C. For the neat EVA-H, we employed only cooling protocol I. We found that the crystallization of the blend and neat EVA-H finished within 3 min at 65°C. After the specimen was kept at 65°C for 20 min, it was heated to 130°C at a rate of 5°C/min to measure  $\Delta H_m$ .

### Phase-Separated Morphology and Phase Diagram

The LLPS morphologies were observed with an optical microscope (OM) (Axioplan, Zeiss Co.). Fresh nitrogen gas was circulated into the heating block attached to the optical microscope to avoid any thermal oxidative degradation. The specimen was prepared by direct pressing of each blend in the molten state without use of a spacer, and the thickness was  $\sim 15$   $\mu\text{m}$ . The determination of the cloud-point temperature ( $T_{cl}$ ) of each

blend has been described elsewhere.<sup>11</sup> The morphology of a specimen after crystallization also was investigated via a polarized mode in the microscope when the temperature was decreased from 130°C to a preset temperature.

### Small-Angle Light Scattering (SALS)

We prepared the sample for the SALS measurement by pressing the sample between two cover glasses at 130°C for 5 min; it then was cooled rapidly to room temperature. The blend composition was 35/65 (wt/wt) EVA-H/wax, the critical composition, and the final film thickness was  $\sim 30$   $\mu\text{m}$ . Two experiments were performed. First, with  $V_v$  optical geometry, an LLPS kinetic experiment at 95°C was carried out for the specimen after the sample was jumped from 130°C. Second, with  $H_v$  optical geometry, a crystallization kinetic experiment at 65°C was investigated for the specimen after the sample experienced three cooling protocols. Here,  $H_v$  optical geometry means that the optical axis of the analyzer was perpendicular to that of the polarizer, and  $V_v$  stands for the optical axis of the analyzer parallel to that of the polarizer. A polarized He–Ne laser with a wavelength of 632.8 nm was placed vertical to the film specimen. The scattering intensities at various  $q$ 's were obtained. Here,  $q$  is the magnitude of the scattering vector,  $q = (4\pi/\lambda) \sin(\theta/2)$ , where  $\lambda$  and  $\theta$  are the wavelength and the scattering angle, respectively.

### Small-Angle X-Ray Scattering (SAXS)

The SAXS measurements with synchrotron radiation were conducted at the 3C2 beam line at the Pohang Light Source, Korea.<sup>12</sup> The primary beam was monochromatized with double  $S_i(111)$  crystals at a wavelength of 0.15402 nm (the photon energy of the X ray was 7.76 keV) and then was focused on a detector plane by a bent cylindrical mirror. A one-dimensional position-sensitive detector (diode-array PSD; Princeton Instruments Inc. Model ST-120) with a distance of 25  $\mu\text{m}$  for

each diode was used. We subtracted the scattering intensity of an empty cell with two pieces of thin polyimide (Kapton) films from that of the samples by taking into account the transmittance of X rays through the samples. The contribution of thermal diffuse scattering (TDS) arising from the density fluctuations was further subtracted. Here, we approximated that the intensity at a higher  $q$  region, where the scattering intensity was independent of  $q$ , was identical to the intensity level of the TDS. The obtained scattering intensities were not converted to the absolute unit. The 35/65 (wt/wt) EVA-H/wax blend with a thickness of 1 mm was cooled to 65°C from 130°C with three cooling protocols. Then, SAXS profiles during the isothermal crystallization at 65°C were measured at every minute up to 20 min. The exposure time was 30 s.

### Rheological Measurement

An advanced Rheometrics expanded system with the dynamic oscillatory mode and parallel plates fixture (25 mm diameter and 1.2 mm gap) was used to monitor change in storage [ $G'(\omega)$ ] and loss modulus [ $G''(\omega)$ ] with phase-separation times. The strain amplitude ( $\gamma_0$ ) and the angular frequency ( $\omega$ ) were kept at 0.03 and 1 rad/s, respectively, which lay in a linear viscoelastic regime. Finally,  $G'(\omega)$  and  $G''(\omega)$  were monitored with crystallization time at 65°C after experiencing three cooling protocols.

## RESULTS AND DISCUSSION

### Phase Behavior

Previously, we reported that the LLPS between the EVA-H and wax occurred at temperatures higher than the melting temperature ( $T_m$ ) of the EVA-H because of the large amount (9.5 wt %) of the polar group of vinyl acetate in the EVA-H, even though the weight-average molecular weight of the wax was just 560.<sup>11</sup> Figure 1 gives the phase diagram of the EVA-H/wax blend obtained from the  $T_{cl}$  of the blend compositions measured by optical microscopy as well as the  $T_m$ 's of the EVA-H and wax in the blend. The  $T_m$ 's were obtained during the second heating at a rate of 10°C/min after the specimens were quenched from 130 to 10°C at a cooling rate of 200°C/min. Thus, the effect of the LLPS on the crystallization of the EVA-H and wax was largely suppressed. From Figure 1, four different regimes existed for

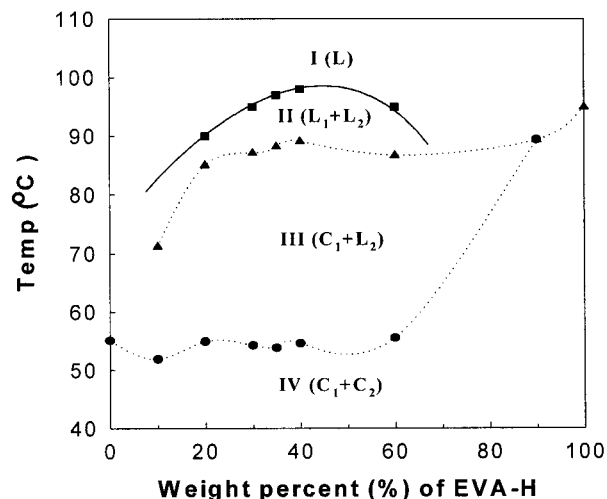


**Figure 1.** Phase diagram of the EVA-H/wax blend<sup>11</sup> (see text for an explanation of each regime). The solid line delineating Regimes I and II is the theoretical binodal curve. ■ =  $T_{ci}$ ; ▲ =  $T_m$  of EVA-H; ● =  $T_m$  of wax.

this blend:<sup>11</sup> Regime I, where the EVA-H and wax were in a homogeneous liquid phase (L); Regime II, where the EVA-H rich phase and the wax-rich phase were phase-separated in a molten state ( $L_1 + L_2$ ), namely the LLPS; Regime III, where the EVA-H was crystallized but wax was still in a molten state ( $C_1 + L_2$ ); and Regime IV, where both the EVA-H and wax were crystallized ( $C_1 + C_2$ ). The solid curve delineating Regime I from Regime II was the predicted binodal curve. From Figure 1, the 35/65 (wt/wt) EVA-H/wax blend became the critical composition, and the temperature range corresponding to the LLPS (or Region II) of this blend was about 10°C. Hereafter, we considered this blend composition only.

Figure 2 gives the one-dimensional  $V_v$  scattering profiles of the 35/65 (wt/wt) EVA-H/wax blend at 95°C with phase-separation time. As the phase-separation time increased, the maximum peak intensity ( $I_m$ ) increased very slowly up to 90 min. However, the maximum peak position ( $q_m$ ) decreased a little at the shorter times, and then it reached a steady value at the longer times. The interdomain spacing ( $\Lambda_{LLPS}$ ) given by  $2\pi/q_m$  was increased a little from 18.9 to 20.8  $\mu\text{m}$  even though the phase-separation time increased from 1 min to 1 h. Therefore, the major increase in  $\Lambda_{LLPS}$  was done within 1 min at 95°C. This is consistent with previous results<sup>11</sup> observed by optical micrography that clearly showed an LLPS proceeding with a self-similarity and 20- $\mu\text{m}$  cocontinuous structures resulting from spinodal de-

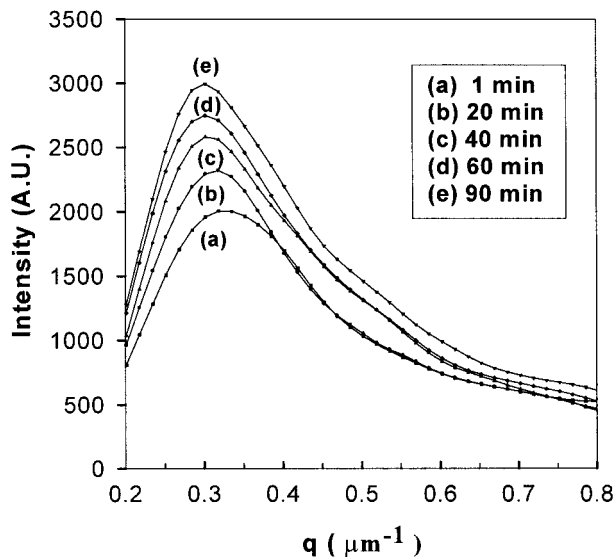


**Figure 2.** Plots of the scattered intensity measured at 95°C versus the wavevector ( $q$ ) with phase-separation time for the 35/65 (wt/wt) EVA-H/wax blend. The time zero is taken as the time when the temperature at the specimen first reached 95°C.

composition. Also, we showed that even if the duration time in the LLPS region increased to 1 h, the  $\Lambda_{\text{LLPS}}$  of the cocontinuous structure increased a little, whereas the concentration difference or the phase contrast became more evident [cf. Fig. 4(b) to Fig. 4(c) in ref. 11]. However, the transition from the cocontinuous structure to the dispersed-domain structure did not occur even if the phase-separation time was increased up to 10 h at 95°C.

Time evolutions of  $G''$  at  $\omega = 1$  rad/s and  $\gamma_0 = 0.03$  and temperature profiles during the experiment are given in Figure 3 when the specimen was quenched from 130 (a homogeneous regime) to 95°C (LLPS regime). It took less than 2 min for temperature stabilization in the rheometer after quenching. We could not measure  $G'$  because of a very low value. It can be seen in Figure 3 that except for the initial increase in  $G''$  resulting from the decrease in the measuring temperature,  $G''$  of the blend did not change with time even though the phase-separation time increased significantly. This is attributed to the fact that as long as cocontinuous morphology is maintained and the domain spacing does not change with time, rheological properties do not change much with phase-separation time.<sup>13</sup>

### Crystallization Behavior

Previously, we reported that the LLPS affected the crystallization behavior of the EVA-H in the

blend.<sup>11</sup> To investigate this effect in detail, we measured the one-dimensional  $H_v$  scattering profiles at the azimuthal angle of 45°. Figure 4 gives plots of the  $H_v$  scattering profiles versus the crystallization time at 65°C after the specimen experienced various cooling histories. With increasing duration in the LLPS regime, the peak position ( $q_m$ ) decreased. However, for each specimen, the  $q_m$  did not decrease with crystallization time. From the  $q_m$ , the radius of the spherulite ( $R_s$ ) is calculated:<sup>14</sup>

$$R_s = 4.09/q_m \quad (1)$$

The  $R_s$  values are given in Table II. The  $R_s$  value of a specimen experiencing an LLPS region at 95°C for 1 h was 10.7  $\mu\text{m}$ , which was almost twice that (5.7  $\mu\text{m}$ ) for another specimen without experiencing LLPS (protocol I). This behavior is consistent with the results of Svoboda et al.,<sup>15</sup> who found that the spherulite size of poly( $\epsilon$ -caprolactone) (PCL) in an 80/20 (wt/wt) PCL/poly(styrene-co-acrylonitrile) (SAN) blend increased with increasing duration time in the LLPS region (or spinodal decomposition time), although the PCL/SAN blend exhibited a lower critical solution temperature (LCST). However, in this study, the diameter of the spherulite in a specimen after experiencing the LLPS region for 1 h was almost the

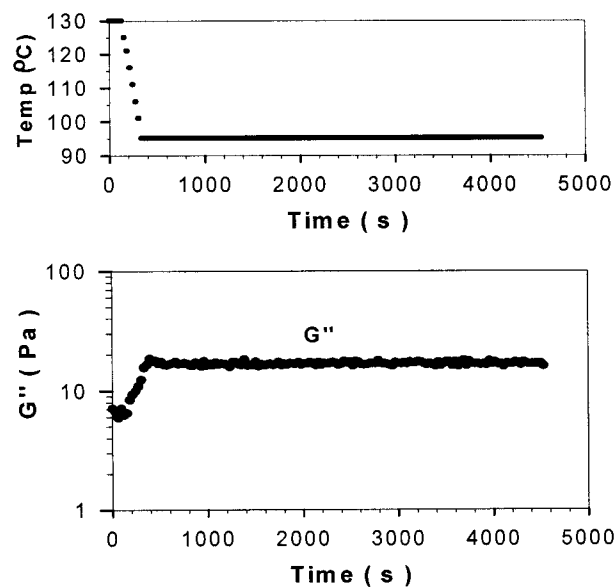


**Figure 3.** Time evolution of  $G''$  at  $\omega = 1$  rad/s and  $\gamma_0 = 0.03$  for the 35/65 (wt/wt) EVA-H/wax blend with an LLPS at 95°C after the blend was direct-quenched from 130 to 95°C. The temperature profile during the experiment is shown in the top panel.

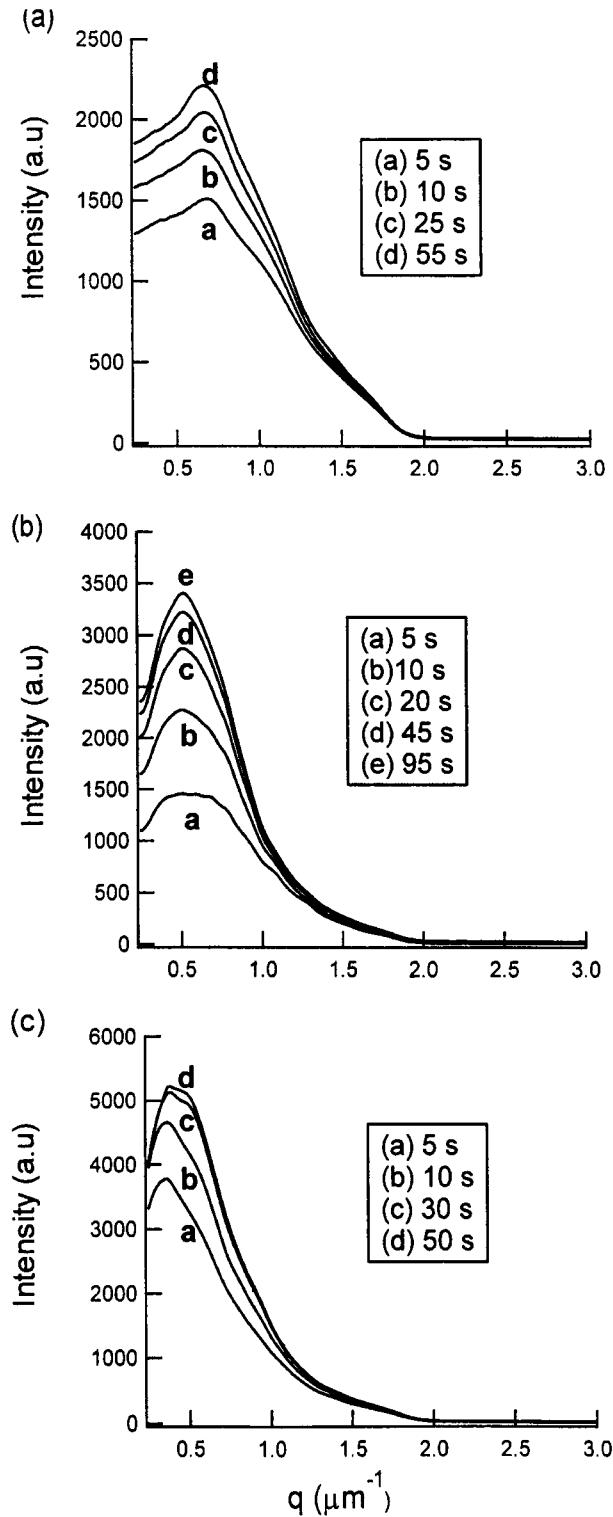


**Figure 4.** One-dimensional  $H_V$  scattering profiles at an azimuthal angle of  $45^\circ$  for the 35/65 (wt/wt) EVA-H/wax blend with a crystallization time at  $65^\circ\text{C}$  after the specimens experienced various cooling histories: (a) protocol I, (b) protocol II, and (c) protocol III. The time zero is taken as the time when the temperature of the specimen first reached  $65^\circ\text{C}$ .

**Table II.** Spherulite Radius ( $R_s$ ) and Order Parameters ( $P_r$ ) of the Lamellae at  $65^\circ\text{C}$  After Various Cooling Histories

Cooling Histories	$R_s$ ( $\mu\text{m}$ )	$P_r$
Protocol I	5.7	3.80
Protocol II	8.2	3.23
Protocol III	10.7	1.84

same as the interdomain spacing ( $\Lambda_{\text{LLPS}}$ ) of cocontinuous structures, whereas that of another specimen after experiencing the LLPS region for 20 min was smaller than the  $\Lambda_{\text{LLPS}}$ , as shown in Table II.

However, the  $I_m$  increased gradually at shorter times and then leveled off within 30 s as shown in Figure 5. It is known that the  $I_m$  of a specimen is proportional to the square of the volume of one spherulite multiplied by the number of spherulites. Also, the number of spherulites is proportional to the inverse of the volume of one spherulite. This implies that  $I_m$  is directly proportional to the volume of one spherulite. The results given in Figure 5 suggest that the volume of one spherulite of a specimen quenched directly from 130 to  $65^\circ\text{C}$  was smaller than that of another experiencing cooling protocols II and III. This is consistent with the results given in Table II and in the OM images given in Figure 6. Furthermore, the initial slope of the maximum intensity normalized by the steady value increased with in-

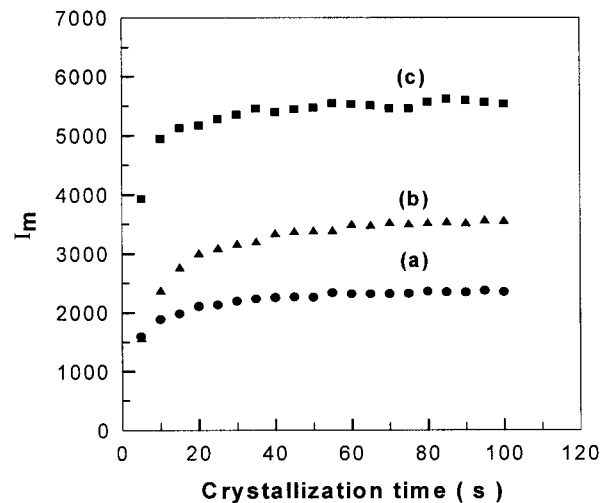


**Figure 5.** The plots of  $I_m$  versus the crystallization time for the 35/65 (wt/wt) EVA-H/wax blend at  $65^\circ\text{C}$  after the specimens experienced three cooling protocols.

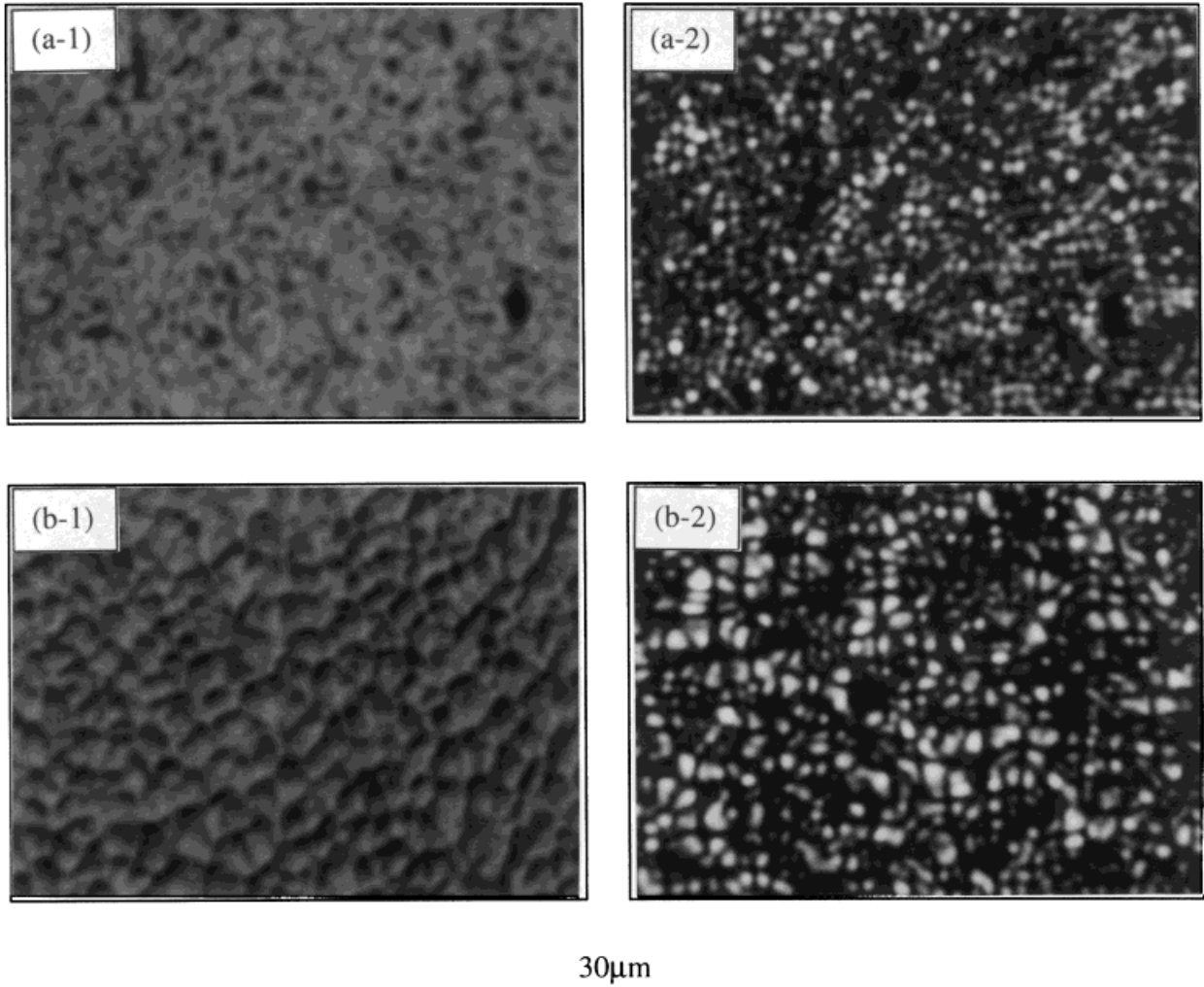


**Figure 6.** OM images in the normal transmission mode (a-1 and b-1) and polarized transmission mode (a-2 and b-2) for the 35/65 (wt/wt) EVA-H/wax blend crystallized at 65°C for 20 min after two cooling histories: (a-1,2) protocol I and (b-1,2) protocol III.

creasing duration time at the LLPS region. Because this slope is proportional to the rate of crystallization, we conclude that the rate of the crystallization became higher with increasing duration time at the LLPS region.

Now, we consider the degree of lamellar ordering in the spherulite (i.e., the order parameter  $P_r$ ) that can be obtained from the one-dimensional  $H_v$  scattering pattern:<sup>16</sup>

$$P_r = I_{Hv}(q_r = 4)/I_{Hv}(q_r = 8) \quad (2)$$

where  $q_r$  is the reduced scattering angle given by

$$q_r = (2\pi/\lambda)R_s \sin \theta \quad (3)$$

The calculated values of  $P_r$  for the specimens after various cooling histories are given in Table II. Interestingly, a specimen quenched directly from 130 to 65°C had a greater lamellar ordering than another specimen after cooling protocols II and III.

Figure 7 gives Lorentz-corrected plots [ $I(q)q^2$  versus  $q$ ] of SAXS profiles for the blend crystallized at 65°C for 20 min after three cooling protocols. Also, those plots are given for the neat EVA-H crystallized at 65°C for 20 min after cooling protocol I. The interlamellar distance or long spacing ( $L = 2\pi/q^*$ , where  $q^*$  is the maximum peak in the Lorentz-corrected plots<sup>3,6,8-10</sup>) for the blend was 1.8 times longer than that of the neat EVA-H, and the intensities at the lower  $q$  for the

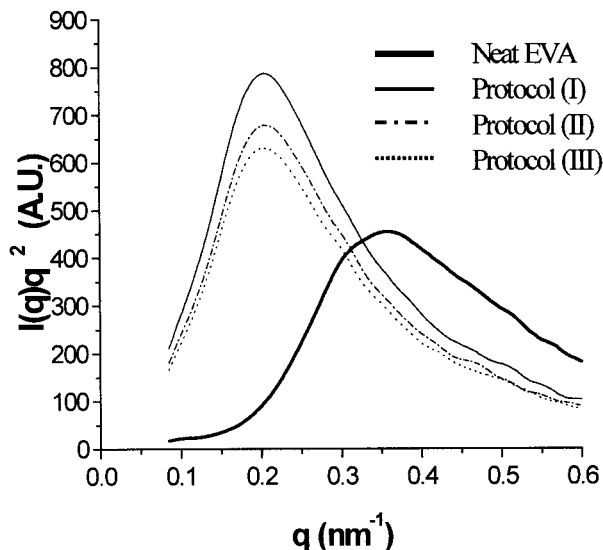


**Figure 7.** Lorentz-corrected SAXS profiles for the 35/65 (wt/wt) EVA-H/wax blend when the specimens were crystallized at 65°C for 20 min after three cooling histories: protocol I (solid curve), protocol II (dashed-dotted curve), and protocol III (dotted curve). Also, plots are given for the neat EVA-H (thick solid curve) crystallized at 65°C for 20 min after cooling protocol I.

blend were higher than those for the neat EVA-H. The SAXS intensity of the neat EVA-H showed a typical peak resulting from the electron density contrast between the alternating crystalline and amorphous phases. The higher intensities at the lower  $q$  for the blend might have been due to the electron density between the lamellar stack domains and the amorphous wax phase. Here, the lamellar stack domains consisted of an EVA-H crystalline phase and the mixed phases of the amorphous part of the EVA-H and molten wax. The results given in Figure 8 have also been seen for a poly(ethylene terephthalate)/poly(ether imide) blend<sup>8</sup> and a poly(3-hydroxy butylate)/poly(vinyl acetate) blend.<sup>9</sup>

In Figure 7, it can be seen that with increasing duration time in the LLPS region, the invariant ( $Q$ ) of the SAXS profiles and  $L$  decreased, although the decrease in  $L$  is not distinct. Here,  $Q$  is defined as follows:<sup>17</sup>

$$Q = \int_0^{\infty} I(q)q^2 dq = \phi_c(1 - \phi_c)\rho_a\rho_c \quad (4)$$

where  $\phi_c$  is the volume fraction of the crystalline phase in the lamellae (or the crystallinity) and  $\rho_c$  and  $\rho_a$  are the densities of the crystalline and

amorphous phases in the lamellae. From eq 4 and Figure 7, one notes that with the increasing duration time in the LLPS region, the crystallinity of the EVA-H decreased because the crystallinity in EVA-H phase was less than 0.5.

To investigate the crystallinity in the EVA-H phase, the thickness of the crystalline phase of EVA-H ( $L_c$ ) in the lamellae and  $L$  were calculated from the one-dimensional correlation function  $\gamma(z)$ :<sup>17</sup>

$$\gamma(z) = \int_0^{\infty} I(q)q^2 \cos(qz) dq / Q \quad (5)$$

The first maximum in  $\gamma(z)$  corresponds to  $L$ , and  $L_c$  (or  $L-L_c$ ) was determined, as shown in Figure 8, depending on the crystallinity of the sample. When the crystallinity is less than 0.5 and the length ratio of  $C$  in Figure 8 divided by  $L$  is less than 0.5, the length  $C$  corresponds to  $L_c$ ; otherwise, the length  $C$  becomes  $L-L_c$ .<sup>17</sup> To determine the crystallinity of the neat EVA-H, we carried out wide-angle X-ray scattering (WAXS) measurement of the neat EVA-H, as shown in Figure 9. From Figure 9, the crystallinity of the EVA-H crystallized at 65°C for 20 min was 0.39. This is consistent with the result reported by Brogly et al.<sup>18</sup> that the crystallinity of an EVA with a vinyl acetate content of 10 wt % was 0.34, as determined by the melting-point depression. Because the linear crystallinity ( $\phi_c^{\text{lin}}$  as given by  $L_c/L$ ) for

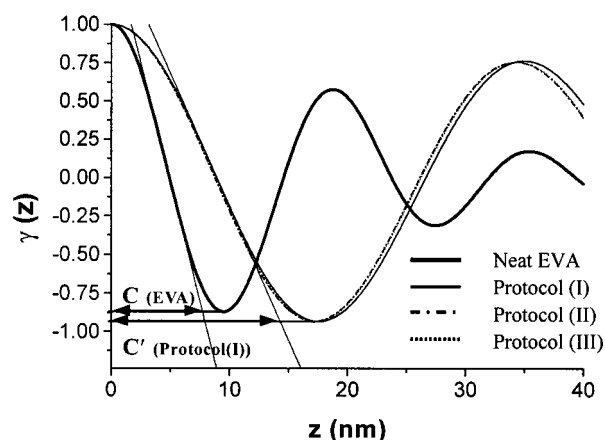


**Figure 8.** One-dimensional correlation function  $\gamma(z)$  for the 35/65 (wt/wt) EVA-H/wax blend when the specimens were crystallized at 65°C for 20 min after three cooling histories: protocol I (solid curve), protocol II (dashed-dotted curve), and protocol III (dotted curve). Also,  $\gamma(z)$  is given for the neat EVA-H (thick solid curve) crystallized at 65°C for 20 min after cooling protocol I.

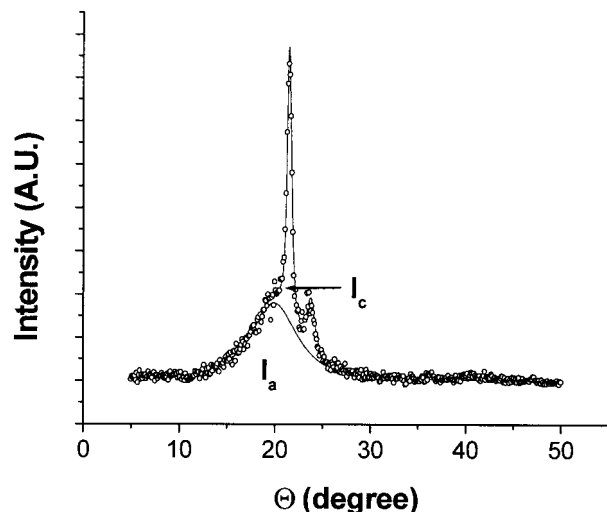


**Figure 9.** WAXS profile of the neat EVA-H crystallized at 65°C for 20 min after being quenched from 130 to 65°C. The crystallinity of the neat EVA-H is obtained from the area ratio of  $I_c$  to the sum of  $I_c + I_a$ .

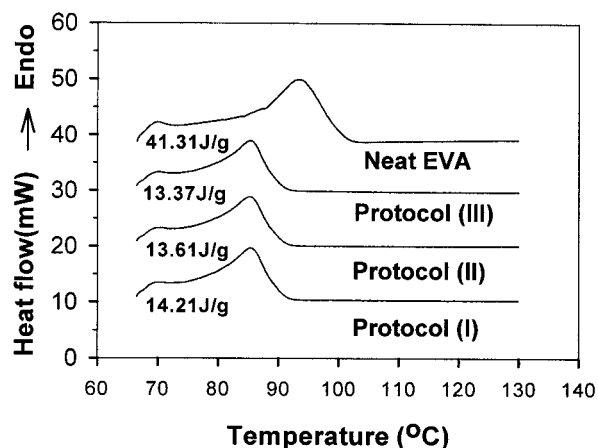
the neat EVA-H was determined to be 0.41 from Figure 8, the length  $C$  in Figure 8 should be equal to  $L_c$ . Similarly, the length  $C'$ , as shown in Figure 8, represents the  $L_c$  of the blend. It is seen in Figure 8 that with increasing duration time in the LLPS region,  $L$  decreased from 35.8 to 34.3 nm, and  $\phi_c^{\text{lin}}$  decreased from 0.42 to 0.41. Furthermore, the thickness of the amorphous phase in the lamellar ( $L-L_c$ ) also slightly decreased with increasing duration time in the LLPS region. These results imply that with increasing duration time at the LLPS, the amount of amorphous molten wax phase located at the amorphous phase of the EVA-H decreased because of the increased segregation between the two phases with the LLPS.

Figure 10 gives DSC thermograms obtained during the heating scan at a rate of 5°C/min from 65 to 130°C for the neat EVA-H and the blends after three cooling protocols. The  $T_m$  of the EVA-H in the blend was 9°C lower than that of the neat EVA-H. The depression of the  $T_m$  was due to the thicker crystalline EVA-H in the lamellae of the blend compared to the neat EVA, as shown in Figure 8. It is well-known that with decreasing  $T_m$ , the degree of supercooling ( $T_m - T_c$ , where  $T_c$  is the crystallization temperature) decreases; therefore, the lamellar thickness increases.<sup>9</sup> With increasing duration time in the LLPS region,  $\Delta H_m$  decreased. These results are consistent with results given in Figure 8. From the DSC results, one can calculate the volume fraction of the lamellar stacking ( $\phi_s$ ), which can be defined as follows:

$$\phi_s = \phi_c / \phi_c^{\text{lin}} \quad (6)$$

where  $\phi_c$  is determined by the bulk crystallinity ( $\Delta H_m / \Delta H_m^0$ , in which  $\Delta H_m^0$  is the heat of melting for 100% of the crystalline EVA-H). From Figures 9 and 10,  $\Delta H_m^0$  was determined to be 98.3 J/g (41.3/0.42). For the neat EVA-H,  $\phi_s$  was about 1.0, implying that the whole sample was homogeneously filled with lamellar stacks. However,  $\phi_s$  for the blends was 0.40 regardless of the cooling protocols. In other words, about 40 volume percents of the sample were filled with lamellar stacks because of the phase separation.

Figure 11 gives time evolutions of  $G'$  and  $G''$  at  $\omega = 1$  rad/s and  $\gamma_o = 0.03$  and temperature profiles during the experiment for specimens after three cooling protocols.  $G'$  and  $G''$  increased dramatically when the temperature was less than the crystallization temperature of the EVA-H in the blend. Furthermore,  $G'$  at the steady state was much larger than  $G''$  because of the existence of the crystallite of the EVA-H. Because the wax was still in an amorphous molten state at 65°C, the rheological behavior of this blend became similar to that of a filled polymer system with inorganic (or organic) filler where the modulus of the filled polymer is proportional to the volume fraction of the filler.<sup>19</sup> Because the EVA-H crystalline phase could be considered the filler,  $G'$  and  $G''$  were proportional to the total volume of the EVA-H crystalline phase and the crystallinity of the EVA-H phase. Interestingly, the steady values of



**Figure 10.** DSC thermograms obtained during heating at a rate of 5°C/min for the 35/65 (wt/wt) EVA-H/wax blend crystallized at 65°C for 20 min after three cooling protocols. Also, a DSC thermogram is given that was obtained during heating at a rate of 5°C/min for the neat EVA-H crystallized at 65°C for 20 min after cooling protocol I.

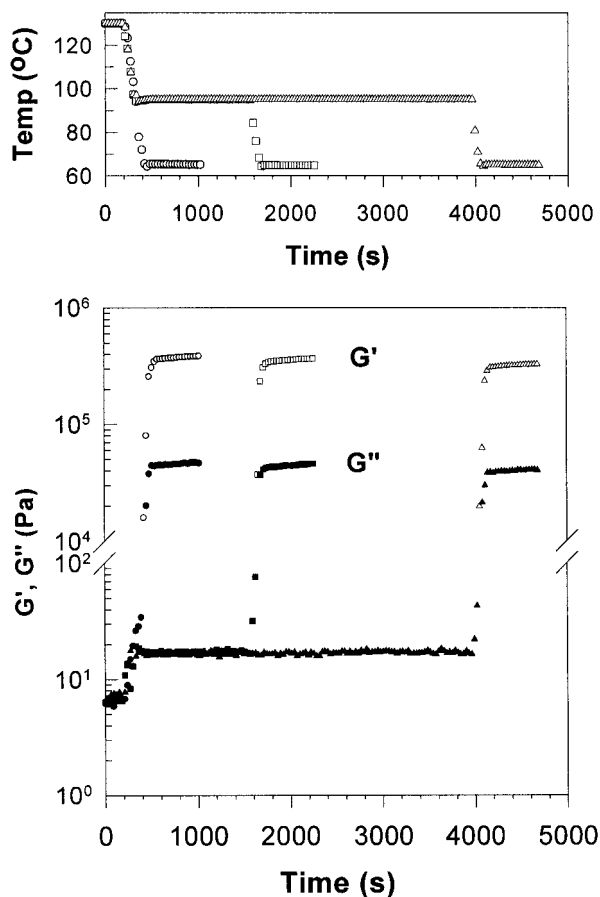


**Figure 11.** Time evolutions of  $G'$  (open symbols) and  $G''$  (filled symbols) at  $\omega = 1$  rad/s and  $\gamma_0 = 0.03$  for the 35/65 (wt/wt) EVA-H/wax blend during crystallization at  $65^\circ\text{C}$  after three different cooling protocols: (○, ●) protocol I, (□, ■) protocol II, and (△, ▲) protocol III. The temperature profiles corresponding to three experimental conditions are shown in the top panel.

$G'$  and  $G''$  at  $65^\circ\text{C}$  slightly decreased with increasing duration time in the LLPS region. This is attributed to the fact that with increased duration time at the LLPS, the crystallinity of the EVA-H phase decreased even though the total volume of the lamellar stacks was almost constant.

## CONCLUSIONS

In this article, we have shown that the LLPS between EVA-H and wax can profoundly affect the crystallization behavior of EVA-H. The critical solution temperature of the blend of the EVA-H and wax was  $98^\circ\text{C}$ . As the duration time in the LLPS region increased before the crystallization at  $65^\circ\text{C}$ , the spherulite size as well as the crystal-

lization kinetics of the EVA-H increased, but the degree of lamellar ordering in the spherulite decreased. The spherulite size became almost the same as the interdomain spacing of the cocontinuous structure formed during the LLPS when the duration time in the LLPS region was increased up to 1 h. Finally, both the degree of the crystallinity of the EVA-H and the interlamellar distance in the blend as well as the moduli decreased with increasing duration time in the LLPS region.

This study was supported in part by a G-7 project (1998) governed by the Ministry of Science and Technology (MOST), Korea. Synchrotron SAXS experiments were performed at the Pohang Light Source (3C2 beam line) in Korea, which was supported by MOST and Pohang Iron & Steel Co. (POSCO).

## REFERENCES AND NOTES

- Avella, M.; Martucelli, E. *Polymer* 1988, 29, 1731.
- Penning, J. P.; Manley, R. J. *Macromolecules* 1996, 29, 77.
- Liu, L. Z.; Chu, B.; Penning, J. P.; Manley, R. J. *Macromolecules* 1997, 30, 4398.
- Isayeva, I.; Kyu, T.; Manley, R. J. *Polymer* 1998, 39, 4599.
- Cham, P. M.; Lee, T. H.; Marand, H. *Macromolecules* 1994, 27, 4263.
- Xing, P.; Ai, X.; Dong, L.; Feng, Z. *Macromolecules* 1998, 31, 6896.
- Chen, C. Y.; Yunus, W. M.; Chien, H. W.; Kyu, T. *Polymer* 1997, 38, 4433.
- Chen, H. L.; Hsiao, M. S. *Macromolecules* 1998, 31, 6579.
- Chiu, H. J.; Chen, H. L.; Lin, T. L.; Lin, J. S. *Macromolecules* 1999, 32, 4969.
- Liu, A. S.; Liao, W. B.; Chiu, W. Y. *Macromolecules* 1998, 31, 6593.
- Kim, J. K.; Kim, B. K. *J Polym Sci Part B: Polym Phys* 1999, 37, 1991.
- Park, B. J.; Rah, S. Y.; Park, Y. J.; Lee, K. B. *Rev Sci Instrum* 1995, 66, 1722.
- Kim, J. K.; Son, H. W.; Lee, Y. B.; Kim, J. *J Polym Sci Part B: Polym Phys* 1999, 37, 889.
- Stein, R. S.; Rhodes, M. J. *J Appl Phys* 1960, 31, 1873.
- Svoboda, P.; Kressler, J.; Inoue, T. *J Macromol Sci Phys* 1996, B35, 505.
- Charoensirisomboon, P.; Saito, H.; Inoue, T. *Macromolecules* 1998, 31, 4963.
- Stroble, G. *The Physics of Polymers*; Springer-Verlag: New York, 1996; Chapter 4.
- Brogly, M.; Nardin, M.; Schultz, J. *J Appl Polym Sci* 1997, 64, 1903.
- Milliken, W. J.; Powell, R. L. In *Flow and Rheology in Polymer Composites Manufacturing*; Advani, S. G., Ed.; Elsevier: New York, 1994; pp 53-83.